

# Supercontinuum Generation by Saturated $\chi^{(2)}$ Interactions

MARC JANKOWSKI<sup>1,2,\*</sup>, CARSTEN LANGROCK<sup>2</sup>, BORIS DESIATOV<sup>3</sup>, MARKO LONČAR<sup>3</sup>, AND M. M. FEJER<sup>2</sup>

<sup>1</sup>NTT Research Inc. Physics and Informatics Labs, 940 Stewart Drive, Sunnyvale, California

<sup>2</sup>Edward L. Ginzton Laboratory, Stanford University, Stanford, California,

<sup>3</sup>John A. Paulson School of Engineering and Applied Sciences, Harvard University, Cambridge, Massachusetts

\*Corresponding author: marc.jankowski@ntt-research.com

Compiled March 1, 2025

**We demonstrate a new approach to supercontinuum generation and carrier-envelope-offset detection in dispersion-engineered nanophotonic waveguides based on saturated second-harmonic generation of femtosecond pulses. In contrast with traditional approaches based on self-phase modulation, this technique simultaneously broadens both harmonics by generating rapid amplitude modulations of the field envelopes. The generated supercontinuum produces coherent carrier-envelope-offset beatnotes in the overlap region that remain in phase across 100's of nanometers of bandwidth while requiring <10 picojoules of pulse energy.** © 2025 Optical Society of America

<http://dx.doi.org/10.1364/ao.XX.XXXXXX>

## INTRODUCTION

The generation of coherent supercontinua from mode-locked lasers is an increasingly important nonlinear process found in many modern optical systems[1–3]. Traditional approaches to supercontinuum generation (SCG) rely on self-phase modulation (SPM) due to  $\chi^{(3)}$  interactions in highly nonlinear fibers or in nanophotonic waveguides, and typically require pulse energies on the order of 100 - 1000 pJ[4]. When used for carrier-envelope-offset (CEO) detection, these devices are followed by a discrete second-harmonic generation (SHG) stage, which frequency doubles the long-wavelength portion of the supercontinuum to overlap with shorter wavelengths and generate an  $f$ - $2f$  beatnote. Recent work has focused on simplifying the operation of these systems, both by reducing the energy required to achieve octave-spanning SCG and by integrating the SHG stage into the same nonlinear waveguide. Energy reductions are typically achieved by fabricating long waveguides that utilize the  $P \propto L^{-1}$  scaling of the necessary power associated with  $\chi^{(3)}$  devices, where  $L$  is the length of the nonlinear waveguide; the current state-of-the-art devices operate with 10's of pJ[5, 6]. Devices with integrated SHG stages typically use parasitic  $\chi^{(2)}$  processes to achieve frequency doubling during spectral broadening[7–11]. This allows for  $f$ - $2f$  beatnotes to be detected from the output of a single nonlinear photonic device. All of these approaches to  $f$ - $2f$  detection typically produce a narrowband second harmonic, which requires the  $f$ - $2f$  beatnotes to be filtered down to a  $\sim$ 10-nm-wide spectral window, thereby limiting the amount of detected photocurrent since only a small fraction of the available

power spectrum is used. Recent work based on SHG in thin-film periodically poled lithium niobate (PPLN) nanophotonic waveguides suggested that these limitations can be overcome by forgoing  $\chi^{(3)}$  processes entirely, and demonstrated the generation of several octaves of bandwidth using 10-pJ of pulse energy[12]. However, to date, the mechanisms responsible for spectral broadening in this system have been poorly understood. We address these questions in this article.

We describe here a new approach to SCG and CEO detection based on saturated second-harmonic generation in a dispersion-engineered thin-film PPLN waveguide. In contrast to traditional approaches based on SPM, this process generates coherent octaves of bandwidth simultaneously for both the fundamental and second harmonic by introducing rapid amplitude modulations onto the pulse envelopes associated with each harmonic. Saturated SHG enables the generation of coherent octaves of bandwidth with substantially lower energy requirements than processes based on  $\chi^{(3)}$  nonlinearities due to both the relative strength and the  $P \propto L^{-2}$  power scaling of  $\chi^{(2)}$  processes. Furthermore, devices based on this process can generate  $f$ - $2f$  beatnotes in the region where the spectra associated with each harmonic overlap. Remarkably, these beatnotes can remain in phase across 100's of nanometers of bandwidth, which enables efficient CEO detection without the need for narrowband filters. The physical processes studied here clarify the behavior of the devices studied in [12], and provide a set of design rules for SCG devices based on saturated  $\chi^{(2)}$  nonlinearities.

This paper proceeds in four sections: 1,2) We develop an

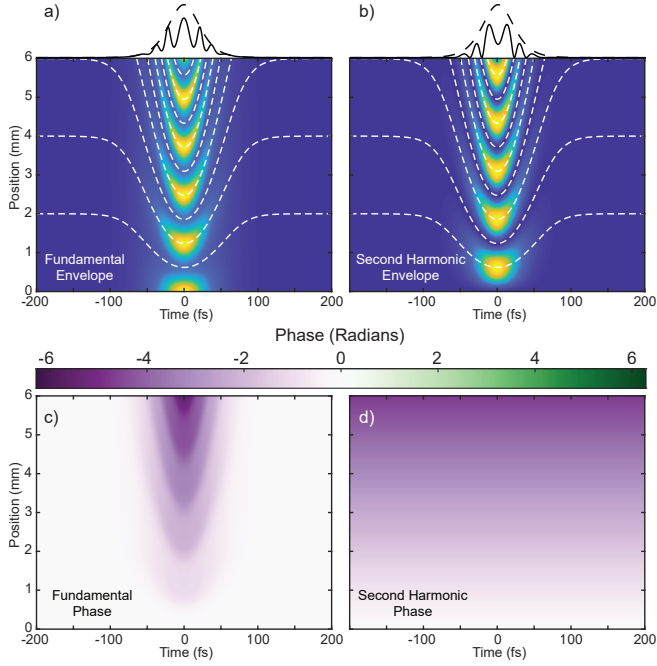


**Fig. 1.** a,b) Theoretical evolution of the fundamental and second harmonic envelopes,  $|A_\omega|^2$  and  $|A_{2\omega}|^2$ . Dashed white lines: conversion half-periods during propagation, dashed black lines: in-coupled fundamental pulse, solid black lines: the resulting pulse at the output of the waveguide for each harmonic. c,d) The phase of the fundamental and second harmonic. The fundamental forms plateaus of constant phase, and the second harmonic exhibits a phase that is independent of time. Spectral broadening is predominantly due to the femtosecond-scale amplitude modulations on each pulse envelope, which can generate coherent octaves of bandwidth.

analytic model of SCG by saturated SHG in the time and frequency domain, respectively, and verify this model using split-step Fourier methods. We then calculate the  $f$ - $2f$  beatnotes in the region of spectral overlap between the two harmonics and show that these beatnotes can remain in phase across broad bandwidths. 3) We summarize the design of the nonlinear waveguides under study and present experimental results, which exhibit good agreement with the theoretical approach established in Sec. 1-2. When driven with 50-fs-long pulses from a 2- $\mu$ m optical parametric oscillator (OPO), these waveguides generate coherent octaves of bandwidth with as little as 4 pJ of pulse energy coupled into the waveguide. 4) We discuss the scalability of this approach, both to lower pulse energies and to longer pulses. This approach to SCG exhibits favorable scaling laws compared to devices based on SPM, and may potentially realize SCG with 100's of femtojoules in cm-scale devices. However, the energy requirements to achieve an octave of bandwidth scale with the cube of the input pulse duration. Therefore, SCG and  $f$ - $2f$  detection using saturated SHG in nanophotonic PPLN waveguides is only practical when the input pulse duration is below 100 fs.

## 1. TIME-DOMAIN THEORY

We consider the evolution of phase-mismatched fundamental and second-harmonic pulses in a dispersion-engineered nanophotonic PPLN waveguide in the limit where the field is sufficiently intense to deplete the fundamental and dispersion

is negligible over the bandwidth of the pulses. This quasi-static model is motivated by several observations[12]: i) previous experimental demonstrations have shown that the generated supercontinua maintain coherence for soliton numbers far in excess of  $\chi^{(3)}$  devices, which suggests that the spectral broadening mechanisms may be different than an effective  $\chi^{(3)}$  due to cascaded  $\chi^{(2)}$  interactions [13–15], ii) the observed relative intensity of the second harmonic violates the assumption of an undepleted fundamental associated with the cascade regime, and iii) the amount of group-velocity dispersion,  $k''_\omega$ , at the fundamental is too small to cause significant self-compression.

The coupled-wave equations for the complex field envelopes  $A_\omega(z, t)$  and  $A_{2\omega}(z, t)$  are given by

$$\partial_z A_\omega = \hat{D}_\omega A_\omega - i\kappa A_{2\omega} A_\omega^* \exp(-i\Delta k z), \quad (1a)$$

$$\partial_z A_{2\omega} = -\Delta k' A_{2\omega} + \hat{D}_{2\omega} A_{2\omega} - i\kappa A_\omega^2 \exp(i\Delta k z), \quad (1b)$$

where  $A_\omega$  is normalized such that  $|A_\omega|^2$  is the instantaneous power of the fundamental wave. The temporal walk-off  $\Delta k' = k'_{2\omega} - k'_\omega$  and dispersion operators  $\hat{D}_\omega = \sum_{j=2}^{\infty} \left[ (-i)^{j+1} k_\omega^{(j)} / j! \right] \partial_t^j$ , where  $k_\omega^{(j)}$  represents the  $j^{\text{th}}$  derivative of propagation constant  $k$  at angular frequency  $\omega$ , are both assumed to be negligible in the quasi-static limit treated here.  $\Delta k = k_{2\omega} - 2k_\omega - 2\pi/\Lambda_G$  is the phase mismatch between the carrier frequencies of the interacting harmonics in the presence of a PPLN grating with period  $\Lambda_G$ , and  $\kappa = \sqrt{2\omega^2 d_{\text{eff}}^2 / (n_\omega^2 n_{2\omega} \epsilon_0 c^3 A_{\text{eff}})} = \sqrt{\eta_0}$  is the nonlinear coupling, where  $\eta_0$  is the conventional normalized SHG efficiency. In this quasi-static limit, Eqns. 1a-1b may be solved for the instantaneous field intensity at each point in time using the Jacobi-Elliptic functions associated with continuous-wave SHG in the limit of a depleted pump[16]. The local instantaneous power of the fundamental and second harmonic are given by

$$|A_\omega(z, t)|^2 = (1 - \eta^2(z, t)) |A_\omega(0, t)|^2, \quad (2a)$$

$$|A_{2\omega}(z, t)|^2 = \eta^2(z, t) |A_\omega(0, t)|^2, \quad (2b)$$

where the instantaneous field conversion efficiency is given by  $\eta(z, t) = v(t) \text{sn}(\kappa A_\omega(0, t) z / v(t) | v^4(t))$ . Here  $\text{sn}$  is the Jacobi elliptic sine and  $v(t) = -|\Delta k / (4\kappa A_\omega(0, t))| + \sqrt{1 + |\Delta k / (4\kappa A_\omega(0, t))|^2}$ .  $v(t)$  represents the maximum pump depletion attainable as a function of the local field amplitude  $A_\omega(0, t)$ .

The Jacobi elliptic solutions found here bear many similarities to the sine-wave evolution that occurs during undepleted phase-mismatched SHG, namely, periodic oscillations of the fundamental and second harmonic power in  $z$ , and a maximum conversion efficiency that increases with increasing pump power. However, the Jacobi-elliptic functions saturate at high power, and the spatial period at which power oscillates between the fundamental and second harmonic, hereafter referred to as the conversion period, decreases as the local field intensity becomes larger. The conversion period varies across the field envelopes as

$$L_{\text{conv}}(t) = 2K(v(t)^4) v(t) / (\kappa A_\omega(0, t)), \quad (3)$$

where  $K$  is the complete elliptic integral of the first kind.  $K(v(t)^4)$  varies slowly for most physically encountered values of  $v(t)$ , e.g.  $K(0) = \pi/2$  and  $K(v^4) \approx 2.3$  for a pump depletion of  $v^2 = 0.9$ , and therefore the variation of  $L_{\text{conv}}(t)$  is dominated by  $v(t) / (\kappa A_\omega(0, t))$ . Fig. 1(a-b) shows the theoretical evolution of a 50-fs-wide  $\text{sech}^2$  pulse in a 6-mm-long waveguide.

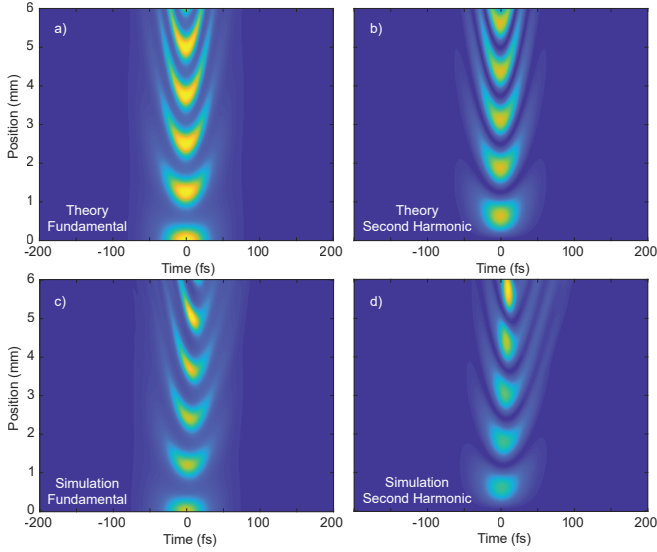


**Fig. 2.** Comparison of quasi-static theory with a full split-step Fourier simulation. a,b) Theoretical fundamental and second harmonic, c,d) simulated fundamental and second harmonic. The structure of the amplitude-modulated harmonics is largely preserved in the presence of moderate amounts of waveguide dispersion.

Here, we have assumed a pulse energy of 4 pJ,  $\eta_0 = 1000 \text{ \%}/\text{W}\cdot\text{cm}^2$ , and  $\Delta k = -3\pi/L$ , where  $L$  is the length of the waveguide. The dotted white lines correspond to the  $m^{\text{th}}$  half-period,  $L_m = mL_{\text{conv}}/2$ , where even  $m$  coincide with the local maxima and minima of the fundamental and second harmonic, respectively. Near the peak of the pulse the conversion period is the shortest and both harmonics undergo  $\sim 5$  conversion periods as the field propagates through the waveguide. The oscillations of the power in the tails of the pulse asymptotically approach to the conversion period associated with undepleted SHG (equal to twice the conventional coherence length in this limit),  $L_{\text{conv}}(\infty) = 2\pi/|\Delta k|$ . Remarkably, the power at the peak oscillates three times faster than in the tails of the pulse, which gives rise to a pulse shape with rapid temporal amplitude oscillations as each portion of the pulse cycles through a different number of conversion periods (Fig. 1, solid lines).

Using the same quasi-static heuristic, the Jacobi elliptic solutions can be shown to predict phase envelopes for the fundamental and second harmonic,

$$\phi_\omega(z, t) = \phi_\omega(0, t) + \frac{\Delta k}{2} \int_0^z \frac{\eta^2(z', t)}{1 - \eta^2(z', t)} dz', \quad (4a)$$

$$\phi_{2\omega}(z, t) = 2\phi_\omega(0, t) - \pi/2 + \frac{\Delta k}{2} z, \quad (4b)$$

respectively, and are plotted in Fig. 1(c,d) for  $\phi_\omega(0, t) = 0$ . The rate of phase accumulation by the fundamental depends strongly on the degree of pump depletion, with large phase shifts accumulated at values of  $z$  and  $t$  that correspond to local maxima of  $\eta(z, t)$ . This behavior results in a saturable effective SPM for the fundamental, with the total accumulated phase plateauing across large time bins (Fig. 1(c)). The phase of the second harmonic is independent of time, and therefore can be neglected in the context of spectral broadening (Fig. 1(d)). These two behaviors suggest that the predominant broadening mechanism for saturated SHG is not effective SPM. Instead, the observed

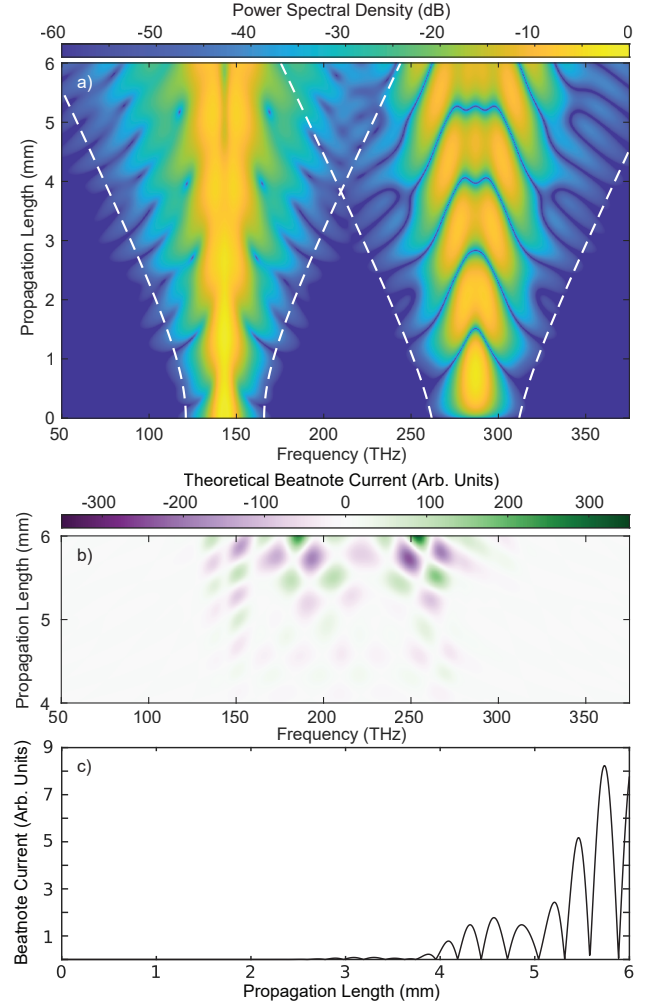


**Fig. 3.** a) Theoretical power spectral density associated with the field envelopes shown in Fig. 1. b) Beatnote photocurrent as a function of frequency and propagation length. The beatnotes periodically fall in- and out-of-phase with propagation length, with some lengths producing beatnotes that remain in-phase across 100's of nm of bandwidth. c) The resulting detected photocurrent oscillates for increasing propagation length due to the periodic re-phasing shown in (b).

spectral broadening of the harmonics is dominated by the rapid amplitude modulations in time accumulated by each pulse.

We now verify this analytic model against a full split-step Fourier model, assuming a temporal walk-off of  $\Delta k' = 5 \text{ fs}/\text{mm}$ , and group velocity dispersion for the fundamental and second harmonic of  $k''_\omega = -15 \text{ fs}^2/\text{mm}$  and  $k''_{2\omega} = 100 \text{ fs}^2/\text{mm}$ , respectively. These values were chosen to correspond to the temporal walk-off and group-velocity dispersion of the TE<sub>00</sub> waveguide modes of the waveguides studied in Sec. III. The time-domain instantaneous power,  $|A_\omega|^2$  and  $|A_{2\omega}|^2$ , is shown in Fig. 2. While the simulated pulse envelopes exhibit some distortion due to second and third-order dispersion, the key aspects of our Jacobi-elliptic approach such as the rapid amplitude modulations of the resulting pulses are largely preserved. Given this strong agreement, we now consider the spectral broadening of the harmonics.

## 2. FREQUENCY-DOMAIN THEORY

Having calculated both the amplitude and phase of each envelope, we may now Fourier transform these envelopes to study the evolution of the power spectral density. While we cannot Fourier transform the fields obtained using Eqns. 2 and 4 analytically, we may gain several insights from the time-domain model that qualitatively capture the behavior of the generated spectrum. First, as noted previously, the phase of the two harmonics has a negligible contribution to spectral broadening, with  $\phi_\omega$  forming plateaus of nearly constant phase and  $\phi_{2\omega}(z, t) = \phi_{2\omega}(z, 0)$  experiencing no time-dependent phase modulation. Second, we note that for  $z > L_{\text{conv}}(0)$  the number of local maxima contained in the instantaneous power of each envelope grows linearly with the number of half-periods around  $t = 0$  and loses two local maxima for every conversion period in the tails of the pulse ( $t \rightarrow \pm\infty$ ). Therefore, the number of local maxima for each harmonic is given by  $N_\omega(z) \approx 2z [L_{\text{conv}}^{-1}(0) - L_{\text{conv}}^{-1}(\infty)]$  and  $N_{2\omega}(z) = N_\omega(z) + 1$  for  $z > L_{\text{conv}}(0)$ ; both harmonics have one local maximum for  $z < L_{\text{conv}}(0)$ . Since the instantaneous power  $|A_\omega(z, t)|^2 + |A_{2\omega}(z, t)|^2$  is conserved, each field envelope effectively bifurcates into  $N$  pulses with a duration  $\sim \tau/N$ , where  $\tau$  is the pulse duration input to the waveguide (e.g.  $\tau_{\text{FWHM}} = 1.76\tau$  for a sech pulse). Based on these observations we expect three behaviors in the frequency domain: i) a bandwidth  $\Delta f$  that grows linearly for  $z$  that satisfy  $N_\omega(z) > 2$  (or  $z \gg L_{\text{conv}}(0)$ ), ii) a constant bandwidth for  $z$  that satisfy  $N_\omega(z) < 2$ , and iii) the appearance of fringes in the frequency domain that become more finely patterned with increasing  $z$ , due to the interference of  $N$  pulses in the time-domain.

The combined power spectral density associated with each harmonic,  $|\hat{A}_\omega(z, \Omega)|^2 + |\hat{A}_{2\omega}(z, \Omega)|^2$  is plotted in Fig. 3(a), for the parameters used in Fig. 1. The white dotted lines correspond to a semi-empirical formula for the spectral half-width based on the arguments made above,

$$\Delta f_\omega(z) = \Delta f(0) \sqrt{1 + (\bar{N}_\omega(z)/2)^2}, \quad (5)$$

where  $\bar{N}_\omega = 2z [z_{\text{NL}}^{-1} - L_{\text{conv}}^{-1}(\infty)]$ ,  $\bar{N}_{2\omega} = \bar{N}_\omega + 1$ , and  $z_{\text{NL}} = \pi\nu(0)/\kappa A_\omega(0, 0)$ . Here  $\Delta f(0)$  was chosen to correspond to the  $-50$  dB level. Eqn. 5 is a reasonable estimate of the spectral broadening due to quasi-static  $\chi^{(2)}$  interactions; we numerically verified that the accuracy of this equation holds as we varied the pulse energy and phase-mismatch over several orders of magnitude. As the field envelopes evolve in the waveguide, the bandwidth associated with each harmonic is observed to be constant for  $z \ll z_{\text{NL}}$ , and to grow linearly for  $z \gg z_{\text{NL}}$ . Furthermore, the power spectral density associated with each harmonic exhibits interference fringes that become more finely patterned with increasing  $z$ , as expected from the qualitative picture discussed previously. We note here that the harmonics merge for  $z > 3.5$  mm, which enables  $f$ - $2f$  interferometry in the region of spectral overlap.

The beatnote power contained in each spectral bin is calculated using  $2\text{Re}(\hat{A}_\omega(z, \Omega)\hat{A}_{2\omega}^*(z, \Omega))$ . Fig. 3(b) shows the calculated  $f_{\text{CEO}}$  beatnote current as a function of frequency for the overlapping spectra. The beatnotes fall in- and out-of phase during propagation, and, remarkably, for a suitable choice of power or device length the  $f_{\text{CEO}}$  beatnotes can remain in-phase across nearly a micron of bandwidth. As shown in Fig. 3(c), this process causes the beatnote current obtained by integrating over the full bandwidth to oscillate depending on the length of the waveguide. In practice, the pulse energy used to drive

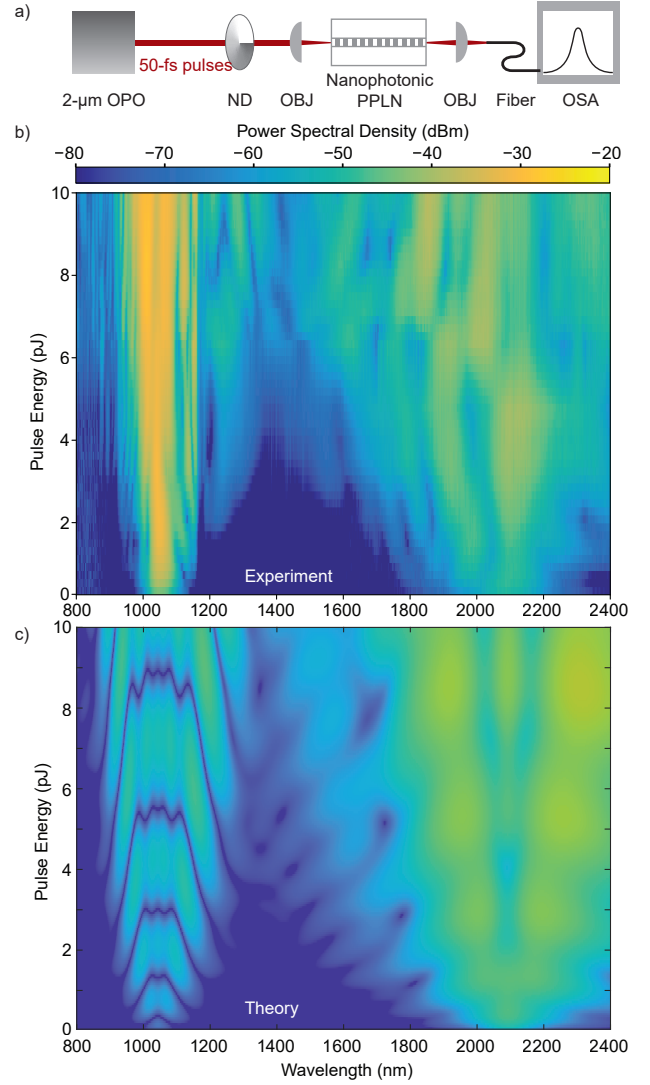


**Fig. 4.** a) Experimental Setup. (OPO) Optical parametric oscillator, (OBJ) metallic cassegrain objective, (OSA) optical spectrum analyzer. b) The experimentally measured and, c) theoretically calculated power spectral density as a function of input pulse energy.

the waveguide can be chosen to align a local maximum of the beatnote current with the length of the device. This process simplifies CEO detection by allowing the output of the waveguide to be focused on a photoreceiver with minimal filtering, while also improving the detected beatnote current by integrating the photocurrent over many comb lines.

## 3. EXPERIMENTAL RESULTS

Having established the physical processes responsible for spectral broadening during saturated SHG, we now experimentally characterize SCG in nanophotonic PPLN devices. The design and fabrication of the devices studied here were reported previously in [12, 17, 18], and we summarize the relevant aspects here. First, we periodically poled a 700-nm-thin film of MgO-doped lithium niobate with 15 poling periods ranging from  $5.01 \mu\text{m}$  to  $5.15 \mu\text{m}$  by applying high voltage pulses to electrodes patterned on the top surface. This shift of 10 nm between

consecutive poling periods corresponds to a shift of the phase mismatch of  $4\pi$ . Fine tuning of the phase-mismatch may be achieved by changing the temperature of the waveguide. Second, waveguides are patterned using electron-beam lithography, and etched into the thin film using  $\text{Ar}^+$  ion-based reactive ion etching. The fabricated waveguides have a top width of  $\sim 1850$  nm and an etch depth of  $\sim 340$  nm, which achieve phasematched SHG of pulses centered around 2060-nm with a poling period of  $\sim 5.11 \mu\text{m}$ .

The experimental setup is shown in Fig. 4(a). The waveguides are driven using 50-fs-long pulses produced with a repetition rate of 100 MHz from a synchronously pumped degenerate optical parametric oscillator. These pulses are coupled into the PPLN waveguides using a reflective inverse-cassegrain objective (Thorlabs LMM-40X-P01). This choice ensures that the incoupled pulses are chirp-free and that the collected harmonics are free of chromatic aberrations. The strongest spectral broadening is observed for a poling period of  $5.10 \mu\text{m}$ , such that  $\Delta kL \sim 3\pi$ . We record the output spectrum from the waveguide using two spectrometers: the near- to mid-infrared (600-1600 nm) is captured with a Yokogawa AQ6370C, and the mid-infrared (1600-2400 nm) is captured using a Yokogawa AQ6375. The results are shown in Fig. 4(b). The fundamental and second harmonic are observed to broaden for input pulse energies in excess of 100 fJ, with the two harmonic merging at the -40 dB level for pulse energies as low as 4-pJ. This observed broadening with increasing pulse energy is consistent with the quasi-static theory shown in Fig. 4(c). Furthermore, we observe a number of qualitative similarities between the spectra observed in theory and experiment. In particular, for pulse energies between one to five picojoules, the power spectrum of the fundamental exhibits a local minimum around the carrier frequency of the fundamental, 2090 nm. For pulse energies greater than five picojoules, this local minimum splits into two minima centered symmetrically around the carrier frequency, with a local maximum at 2090 nm. Similar patterns occur in the tails of the spectra; the spectrum of the fundamental forms successive local minima and maxima in the band between 1600 - 1800 nm with increasing pulse energy, and the second harmonic exhibits oscillatory tails between 1200 - 1400 nm. However, the experimentally observed second harmonic is much brighter than the theoretical predictions made here.

For energies  $>5$  pJ,  $f-2f$  beatnotes may be detected in the region of spectral overlap by filtering the light output from the waveguide and focusing it onto a photodiode (Fig. 5(a)). Fig. 5(b) shows the theoretical beatnote contrast output from the waveguide,  $2\text{Re}(\hat{A}_\omega(L, \lambda)\hat{A}_{2\omega}^*(L, \lambda)) / (|\hat{A}_\omega(L, \lambda)|^2 + |\hat{A}_{2\omega}(L, \lambda)|^2)$ , as a function of wavelength and pulse energy. The contrast is highest in the spectral region from 1200 - 1800 nm. Therefore, we detect  $f-2f$  beatnotes by filtering the light output from the waveguide using a Thorlabs FELH1250 longpass filter, and focus this light on a MenloSystems APD310 avalanche photodiode. We record the RF beatnotes using a Rigol DSA815 RF spectrum analyzer with the resolution bandwidth set to 10 kHz. The RF beatnote power in dBm is shown in Fig. 5(c) as a function of input pulse energy. We observe oscillations of the beatnote power with increasing pulse energy, which is consistent with periodic re-phasing of the beatnotes predicted by theory (Fig. 5(c), dashed line). The beatnote current achieves a local maximum around an input pulse energy of 9.75 pJ, and we obtain an RF beatnote power of -65 dBm. Fig. 5(d) compares the relative intensity of the measured  $f_{\text{CEO}}$  beatnote with the  $f_R$  beatnote corresponding to the repetition rate of the pulses for a pulse

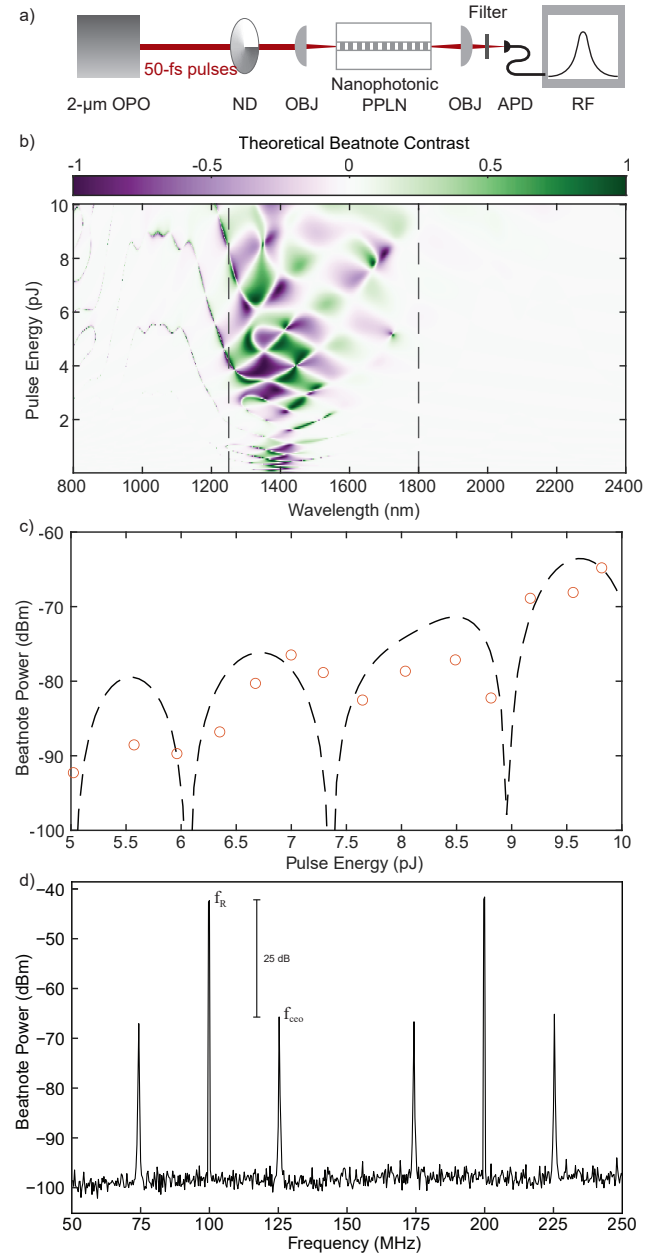


**Fig. 5.** a) Experimental Setup. (APD) Avalanche photodiode, (RF) Radiofrequency spectrum analyzer. b) Theoretical beatnote contrast as a function of wavelength and pulse energy. Based on this calculation, we detect the range from 1250 nm - 1800 nm (dashed grey lines) using a long-pass filter and an InGaAs avalanche photodiode. c) Measured beatnote power as a function of pulse energy. Orange circles correspond to experiment, and the dashed black line corresponds to theory. d) Measured  $f-2f$  beatnotes, for a pulse energy of  $\sim 10$  pJ.

energy of 9.75 pJ. The detected  $f_{\text{CEO}}$  beatnote power is only 25 dB below the  $f_R$  beatnote, even when the detected optical bandwidth spans  $\sim 550$  nm.

#### 4. SCALABILITY OF THIS APPROACH

In practice, there are two main considerations that determine how well this technique performs relative to conventional ap-

proaches, namely, i) the power requirements and ii) the pulse duration requirements necessary to achieve octaves of bandwidth. We first consider the energy requirements of SCG by saturated  $\chi^{(2)}$  nonlinearities using Eqn. 1, and compare the resulting scaling laws against traditional approaches to SCG based on soliton fission in waveguides with  $\chi^{(3)}$  nonlinearities. Eqns. 1 are scale invariant when  $z \rightarrow s_1 z$ ,  $\Delta k \rightarrow \Delta k/s_1$ ,  $\Delta k' \rightarrow \Delta k'/s_1$ ,  $\hat{D}_\omega \rightarrow \hat{D}_\omega/s_1$ ,  $\hat{D}_{2\omega} \rightarrow \hat{D}_{2\omega}/s_1$ , and  $P_{\text{in}}(t) = |A_\omega(0,t)|^2 + |A_{2\omega}(0,t)|^2 \rightarrow P_{\text{in}}(t)/s_1^2$ . Therefore, an increase of device length by a factor  $s_1$  correspondingly results in a quadratic reduction of the pulse energy necessary to achieve the same degree of spectral broadening at the output,  $U_{\text{in}} \rightarrow U_{\text{in}}/s_1^2$ , provided that the dispersion of the waveguide remains sufficiently negligible over the length of the device. In contrast, the nonlinear Schrödinger equation used to describe SCG in waveguides with  $\chi^{(3)}$  nonlinearities is scale invariant when  $z \rightarrow sz$ ,  $\hat{D} \rightarrow \hat{D}/s$ , and  $P_{\text{in}}(t) \Rightarrow P_{\text{in}}(t)/s$ , which exhibits a linear reduction of the energy required to produce a supercontinuum as the length of the waveguide is increased. While state-of-the-art devices based on  $\chi^{(3)}$  nonlinearities have been able to achieve SCG with 10's of pJ using long waveguides, the quadratic scaling of the energy requirements associated with a  $\chi^{(2)}$  process may enable octave-spanning SCG with 100's of femtojoules of pulse energy by rescaling the waveguide designs shown here to centimeters.

We now consider the role of pulse duration by using Eqn. 5. In the limit of large nonlinear coupling ( $\kappa A_\omega(0,0) \gg \Delta k$ ), or large  $z$ , the bandwidth grows as  $\Delta f(z) = \Delta f(0)\kappa A_\omega(0,0)z/\pi$ . Rescaling the input pulse duration by a factor  $s_2$  reduces both the input bandwidth and intensity,  $\Delta f(0) \rightarrow \Delta f(0)/s_2$  and  $A_\omega(0,0) \rightarrow A_\omega(0,0)/\sqrt{s_2}$ , such that power required to achieve a desired  $\Delta f$  increases as  $U_{\text{in}} \rightarrow U_{\text{in}}s_2^3$ . The cubic scaling derived here is shown in Fig. 6, where the spectral broadening of a 4-pJ, 50-fs pulse is compared against a 4-nJ, 500-fs pulse, with each achieving a similar amount of bandwidth at the output. This cubic scaling restricts us to pulse durations on the order of  $\leq 100$  fs simply because the energy requirements of longer pulses are impractical. Even a 200-fs-long pulse would require 100's of picojoules of pulse energy to achieve the output bandwidths demonstrated here, whereas similar pulse energies have already been used to produce  $\chi^{(3)}$  supercontinua in LN nanowaveguides [10, 19]. While these limitations can be overcome by using longer waveguides or more tightly confining (and therefore more nonlinear) geometries, care must be taken to ensure that the nonlinear coupling is sufficient to produce octaves of bandwidth when using pulses with a longer duration.

## 5. CONCLUSION

We have established a theoretical model of supercontinuum generation based on saturated quasi-static  $\chi^{(2)}$  interactions, and have experimentally verified this model by studying spectral broadening in PPLN nanowaveguides. In contrast with the effective self-phase modulation that occurs with cascaded  $\chi^{(2)}$  interactions, here spectral broadening occurs due to rapid amplitude modulations across the pulse envelope of the fundamental and second harmonic. This process generates coherent octaves of bandwidth with picojoules of pulse energy, and produces  $f$ - $2f$  beatnotes that can remain in-phase across 100's of nanometers of bandwidth. This behavior simplifies  $f$ - $2f$  detection and improves the signal-to-noise ratio of the detected  $f_{\text{CEO}}$  beatnote since the detected photocurrent can be integrated over many

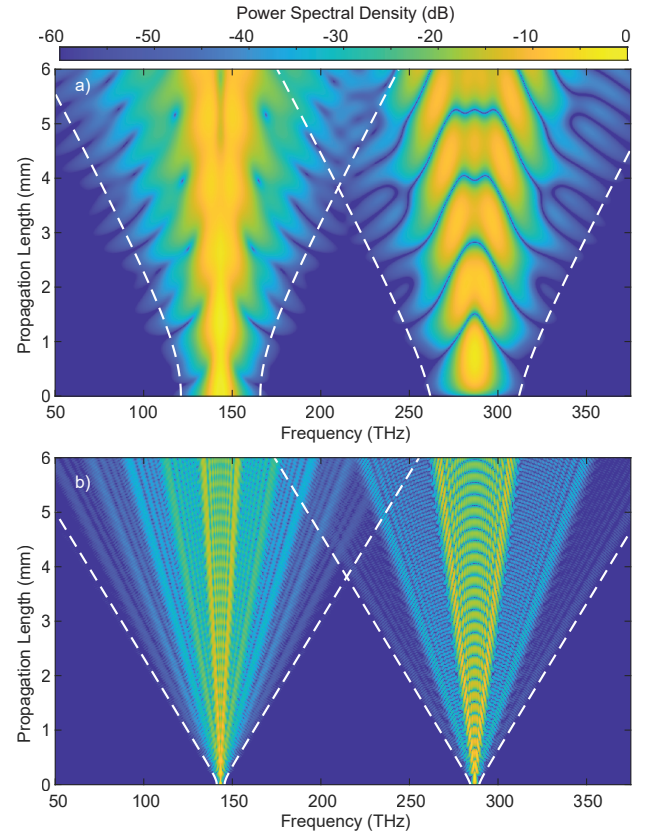


**Fig. 6.** Theoretical broadening of a) a 50-fs-long, 4-pJ pulse, and b) a 500-fs-long, 4-nJ pulse. Dashed white lines correspond to Eqn. 5. For  $z \gg L_{\text{conv}}(0)$  the spectra grow linearly with  $z$ , and achieve a similar output bandwidth. This cubic scaling of necessary pulse energy with input pulse duration limits this technique to pulses with a duration  $\leq 100$  fs.

comb lines. Finally, we use our model to derive a set of scaling laws that provide simple design rules for devices based on saturated  $\chi^{(2)}$  interactions.

**Funding Information.** National Science Foundation (NSF) (ECCS-1609549, ECCS-1609688, EFMA-1741651); AFOSR MURI (FA9550-14-1-0389); Army Research Laboratory (ARL) (W911NF-15-2-0060, W911NF-18-1-0285).

**Acknowledgments.** The authors wish to thank NTT Research for their financial and technical support. Electrode patterning and poling was performed at the Stanford Nanofabrication Facility, the Stanford Nano Shared Facilities (NSF award ECCS-2026822), and the Cell Sciences Imaging Facility (NCRR award S10RR02557401). Patterning and dry etching was performed at the Harvard University Center for Nanoscale Systems (CNS), a member of the National Nanotechnology Coordinated Infrastructure (NNCI) supported by the National Science Foundation. The authors thank Jingshi Chi at DISCO HI-TEC America for her expertise with laser dicing lithium niobate.

**Disclosures.** The authors declare no conflicts of interest.

**Data availability.** Data underlying the results presented in this paper may be obtained from the authors upon request.

## REFERENCES

1. J. Ye and S. T. Cundiff, eds., *Femtosecond Optical Frequency Comb: Principle, Operation, and Applications* (Springer, Boston, MA, 2005).

2. S. A. Diddams, "The evolving optical frequency comb [invited]," *J. Opt. Soc. Am. B* **27**, B51 (2010).
3. N. Picqué and T. W. Hänsch, "Frequency comb spectroscopy," *Nat. Photonics* **13**, 146–157 (2019).
4. J. M. Dudley, G. Genty, and S. Coen, "Supercontinuum generation in photonic crystal fiber," *Rev. Mod. Phys.* **78**, 1135–1184 (2006).
5. A. S. Mayer, A. Klenner, A. R. Johnson, K. Luke, M. R. E. Lamont, Y. Okawachi, M. Lipson, A. L. Gaeta, and U. Keller, "Frequency comb offset detection using supercontinuum generation in silicon nitride waveguides," *Opt. Express* **23**, 15440 (2015).
6. L. M. Krüger, A. S. Mayer, Y. Okawachi, X. Ji, A. Klenner, A. R. Johnson, C. Langrock, M. Fejer, M. Lipson, A. L. Gaeta, V. J. Wittwer, T. Sūd-meyer, C. R. Phillips, and U. Keller, "Self-referenced CEO frequency detection of a 10-GHz laser enabled by highly efficient nonlinear waveguides," in *Laser Congress 2020 (ASSL, LAC)*, (OSA, 2020).
7. D. R. Carlson, D. D. Hickstein, A. Lind, S. Droste, D. Westly, N. Nader, I. Coddington, N. R. Newbury, K. Srinivasan, S. A. Diddams, and S. B. Papp, "Self-referenced frequency combs using high-efficiency silicon-nitride waveguides," *Opt. Lett.* **42**, 2314 (2017).
8. Y. Okawachi, M. Yu, J. Cardenas, X. Ji, A. Klenner, M. Lipson, and A. L. Gaeta, "Carrier envelope offset detection via simultaneous supercontinuum and second-harmonic generation in a silicon nitride waveguide," *Opt. Lett.* **43**, 4627 (2018).
9. D. D. Hickstein, D. R. Carlson, H. Mundoor, J. B. Khurgin, K. Srinivasan, D. Westly, A. Kowligy, I. I. Smalyukh, S. A. Diddams, and S. B. Papp, "Self-organized nonlinear gratings for ultrafast nanophotonics," *Nat. Photonics* **13**, 494–499 (2019).
10. M. Yu, B. Desiatov, Y. Okawachi, A. L. Gaeta, and M. Lončar, "Coherent two-octave-spanning supercontinuum generation in lithium-niobate waveguides," *Opt. Lett.* **44**, 1222 (2019).
11. Y. Okawachi, M. Yu, B. Desiatov, B. Y. Kim, T. Hansson, M. Lončar, and A. L. Gaeta, "Chip-based self-referencing using integrated lithium niobate waveguides," *Optica* **7**, 702 (2020).
12. M. Jankowski, C. Langrock, B. Desiatov, A. Marandi, C. Wang, M. Zhang, C. R. Phillips, M. Lončar, and M. M. Fejer, "Ultrabroadband nonlinear optics in nanophotonic periodically poled lithium niobate waveguides," *Optica* **7**, 40 (2020).
13. M. Bache, "Cascaded nonlinearities for ultrafast nonlinear optical science and applications," Habilitation thesis, Technical University of Denmark (2017).
14. R. DeSalvo, H. Vanherzeele, D. J. Hagan, M. Sheik-Bahae, G. Stegeman, and E. W. V. Stryland, "Self-focusing and self-defocusing by cascaded second-order effects in KTP," *Opt. Lett.* **17**, 28 (1992).
15. C. Conti, S. Trillo, P. D. Trapani, J. Kilius, A. Bramati, S. Minardi, W. Chinnaglia, and G. Valiulis, "Effective lensing effects in parametric frequency conversion," *J. Opt. Soc. Am. B* **19**, 852 (2002).
16. J. A. Armstrong, N. Bloembergen, J. Ducuing, and P. S. Pershan, "Interactions between light waves in a nonlinear dielectric," *Phys. Rev.* **127**, 1918–1939 (1962).
17. M. Zhang, C. Wang, R. Cheng, A. Shams-Ansari, and M. Lončar, "Monolithic ultra-high-q lithium niobate microring resonator," *Optica* **4**, 1536 (2017).
18. C. Wang, C. Langrock, A. Marandi, M. Jankowski, M. Zhang, B. Desiatov, M. M. Fejer, and M. Lončar, "Ultrahigh-efficiency wavelength conversion in nanophotonic periodically poled lithium niobate waveguides," *Optica* **5**, 1438 (2018).
19. J. Lu, J. B. Surya, X. Liu, Y. Xu, and H. X. Tang, "Octave-spanning supercontinuum generation in nanoscale lithium niobate waveguides," *Opt. Lett.* **44**, 1492 (2019).